

Magnetocrystalline anisotropy energy of transition-metal thin films: A nonperturbative theory

A. Lessard, T. H. Moos, and W. Hübner

Institute for Theoretical Physics, Freie Universität Berlin, Arnimallee 14, D-14 195 Berlin, Germany

(Received 27 August 1996; revised manuscript received 24 March 1997)

The magnetocrystalline anisotropy energy E_{anis} of free-standing monolayers and thin films of Fe and Ni is determined using two different semiempirical schemes. Within a *tight-binding calculation* for the $3d$ bands alone, we analyze in detail the relation between band structure and E_{anis} , treating spin-orbit coupling (SOC) nonperturbatively. We find important contributions to E_{anis} due to the lifting of band degeneracies near the Fermi level by SOC. The important role of degeneracies is supported by the calculation of the electron temperature dependence of the magnetocrystalline anisotropy energy, which decreases with the temperature increasing on a scale of several hundred K. In general, E_{anis} scales with the square of the SOC constant λ_{so} . Including $4s$ bands and s - d hybridization, the *combined interpolation scheme* yields anisotropy energies that quantitatively agree well with experiments for Fe and Ni monolayers on Cu(001). Finally, the anisotropy energy is calculated for systems of up to 14 layers. Even after including s bands and for multilayers, the importance of degeneracies persists. Considering a fixed fct-Fe structure, we find a reorientation of the magnetization from perpendicular to in-plane at about 4 layers. For Ni, we find the correct in-plane easy axis for the monolayer. However, since the anisotropy energy remains nearly constant, we do not find the experimentally observed reorientation. [S0163-1829(97)00629-2]

I. INTRODUCTION

The dependence of the total energy of a ferromagnetic crystal on the direction of magnetization originates from the magnetic dipole-dipole interaction as well as from spin-orbit coupling (SOC), as proposed by van Vleck.¹ The magnetic anisotropy energy is expected to be enlarged in systems of low symmetry, i.e., at surfaces, interfaces, and thin films² or in one-dimensional systems such as quantum corrals.³ Recently, a magnetization easy-axis perpendicular to the film plane has been observed for a wide variety of thin film systems, for example for thin films of fcc Fe on Cu(001).⁴⁻⁶ Some of these systems are promising candidates for magnetic high-density storage media.

In spite of many theoretical attempts,⁷⁻¹⁵ the relationship between the electronic structure and magnetocrystalline anisotropy energy E_{anis} could not be fully clarified so far. Some very important questions are subject to intense discussion. (i) Which band structure details lead to significant contributions to E_{anis} ? Especially the treatment of degenerate bands near the Fermi level has brought up controversies.¹¹⁻¹³ (ii) How does E_{anis} depend on the SOC strength λ_{so} ? (iii) How is it influenced by the substrate lattice constant? Moreover, there is no unified thermodynamic and electronic theory to determine the temperature dependence of E_{anis} . Finally, the correct prediction of magnetic anisotropy for real systems still remains a challenge, since due to the quenching of orbital angular momentum in $3d$ transition metal systems, E_{anis} is several orders of magnitude smaller than other contributions to the total energy of a crystal (typically about 0.1–1 meV per atom in ultrathin films).

The magnetic anisotropy of thin films has been investigated using two essentially different approaches. In semiempirical calculations,^{7,8,10,14} the magnetocrystalline anisotropy energy E_{anis} is determined by means of parametrized tight-binding band structures. Usually, spin-orbit coupling is

restricted to second-order perturbation theory. On the other hand, *ab initio* calculations have been made^{9,12,13,15} and lead to realistic band structures. Most calculations make use of the controversial force theorem.¹⁶ Convergence, however, is difficult to achieve; sometimes, additional assumptions are made in order to obtain converged results (*state tracking method*).¹²

The structure of thin Fe films deposited on Cu(001) has been widely investigated, especially the dependence of the structure and magnetization orientation on the temperature. For films of less than 5 monolayers (ML) deposited at low temperatures, a distorted fcc structure is found, with magnetization perpendicular to the film plane. At 5 ML, a transition to in-plane magnetization is observed, as well as a restructuring of the film. It is still not clear if this reorientation transition is an effect of the structural changes taking place in the film at 4–5 ML.^{5,17-20}

In this paper, we investigate a simple quadratic Fe and Ni monolayer and fcc multilayer systems up to 14 ML epitaxially grown on the Cu(001) surface and neglect further interactions with the substrate. The band structures are calculated within two different semiempirical schemes, including SOC completely nonperturbatively without resorting to degenerate or nondegenerate perturbation theory of any order. A *tight-binding calculation* of the $3d$ bands allows for a detailed, \mathbf{k} -space resolved analysis of the role of degeneracies for E_{anis} . It is shown that degeneracies located near the Fermi level can yield significant contributions, if they occur along *lines* in \mathbf{k} space. We find for these that generally $E_{\text{anis}} \propto \lambda_{\text{so}}^2$ holds. Including $4s$ bands by means of the *combined interpolation scheme*²¹ and fitting the parameters to *ab initio* calculations, we obtain the correct sign and values of E_{anis} for the systems considered with this fully convergent method. That could be achieved neither by a fit using bulk parameters nor by employing a real-space density of states calculation, the so-called recursion method.¹¹ Moreover, we find the

characteristic scale for the temperature dependence of the magnetic anisotropy to be λ_{so} , rather than the bandwidth. This supports the significance of the lifting of degeneracies at E_F by λ_{so} and demonstrates the importance of contributions to magnetic anisotropy due to Fermi-edge smearing.

Finally, we calculate the anisotropy energy of multilayer systems. For systems of tetragonally distorted Fe of 2 to 14 ML, we find a transition from magnetization perpendicular to the plane to in-plane magnetization at about 4 ML. We conclude from our calculation that the experimentally observed reorientation at five layers is not necessarily caused by a structural phase transition. For Ni, we find a nearly constant anisotropy energy from the fourth layer on, in disagreement with the results of Schulz and Baberschke,²² who find a reorientation from in-plane to parallel magnetization at 7 ML. In both cases, the degeneracies near the Fermi level are found to play an important role for the dependence of the anisotropy energy on the film thickness.

This paper is organized as follows. In Section II, the interpolation schemes (II A, II B, II C) and the determination of E_{anis} (II D) are presented. The results obtained from the tight-binding scheme for d bands alone are shown in Sec. III A, the role of degeneracies is analyzed in detail in Sec. III B while the results for the complete s - and d -band calculation for Fe and Ni monolayers on Cu(001) and other substrates are given in Sec. III C. The influence of crystal field splitting is investigated. Some aspects of the temperature dependence of magnetic anisotropy are considered in Sec. III D, and the results for multilayer systems are presented in Secs. III E and III F. Section IV sums up the most important results.

II. THEORY

A. Band structures

The magnetocrystalline anisotropy energy E_{anis} depends sensitively on the electronic structure of the system. To simplify the analysis, the band structure of the monolayer is calculated in two steps. First, the $3d$ bands are described within a tight-binding scheme. Although the resulting E_{anis} as a function of the $3d$ -band filling n_d shows already the most important features, the $4s$ bands and s - d hybridization have to be taken into account for a correct numerical evaluation of E_{anis} .

For the $3d$ bands, the tight-binding formalism introduced by Fletcher²³ and Slater and Koster²⁴ is adapted to the monolayer. The Hamiltonian $H^d = H_{\text{at}} + \Delta U$ is set up as a 10×10 matrix with respect to the basis of Bloch wave functions

$$\psi_{\mathbf{n}\mathbf{k}}(\mathbf{r}) = \frac{1}{\sqrt{N}} \sum_{\mathbf{R}} e^{i\mathbf{k} \cdot \mathbf{R}} \phi_{\mathbf{n}}(\mathbf{r} - \mathbf{R}). \quad (1)$$

Here, H_{at} is the atomic Hamiltonian, ΔU the additional crystal field in the monolayer. ϕ_i , $i = 1, \dots, 5$ ($i = 6, \dots, 10$) are the atomic $3d$ orbitals commonly denoted by xy , yz , zx , $x^2 - y^2$, and $3z^2 - r^2$, respectively, together with the spin eigenstate $|\uparrow\rangle$ ($|\downarrow\rangle$) with respect to the spin quantization axis z_M . In the simple quadratic monolayer, only orbitals located on neighboring atoms are included. The extension to second nearest neighbors does not lead to further insight.²⁵ With the

x and y axes oriented along axes connecting nearest neighbors in the monolayer, the spin-polarized Hamilton matrix has (within the three-center approximation) the form

$$\begin{aligned} H_{11}^d &= E_0 + \Delta_{\text{Ni}}^V + 2\tilde{B}_1(\cos 2\xi + \cos 2\eta) - J_{\text{ex}}/2, \\ H_{22}^d &= E_0 + 2\tilde{B}_2 \cos 2\xi + 2\tilde{B}_3 \cos 2\eta - J'_{\text{ex}}/2, \\ H_{33}^d &= E_0 + 2\tilde{B}_3 \cos 2\xi + 2\tilde{B}_2 \cos 2\eta - J'_{\text{ex}}/2, \end{aligned} \quad (2)$$

$$H_{44}^d = E_0 + \Delta_{\text{Fe}}^V + 2\tilde{B}_4(\cos 2\xi + \cos 2\eta) - J'_{\text{ex}}/2,$$

$$H_{55}^d = E_0 + \Delta_{\text{Ni}}^V + \Delta_{\text{Fe}}^V + 2\tilde{B}_5(\cos 2\xi + \cos 2\eta) - J_{\text{ex}}/2,$$

$$H_{45}^d = H_{54}^d = H_{9,10}^d = H_{10,9}^d = 2\tilde{B}_6(\cos 2\xi - \cos 2\eta),$$

and

$$H_{ii}^d = H_{i-5,i-5}^d + J_{\text{ex}} \quad \text{for } i = 6, 10,$$

$$H_{ii}^d = H_{i-5,i-5}^d + J'_{\text{ex}} \quad \text{for } i = 7, 8, 9.$$

Here, $\xi = \frac{1}{2}k_x a$ and $\eta = \frac{1}{2}k_y a$ are the normalized components of the crystal momentum \mathbf{k} , a is the lattice constant of the simple quadratic monolayer. For qualitative results it is sufficient to use bulk values for the parameters of the paramagnetic band structure \tilde{B}_i , the crystal field parameter $\Delta_{\text{Fe/Ni}}^V$, and the spin splitting parameters J_{ex} and J'_{ex} . For Ni, the parameters are taken from Weling and Callaway,^{26,27} for Fe from Pustogowa *et al.*^{28,29} The \tilde{B}_i and Δ^V are listed in the first column of Table I. We have used $J_{\text{ex}} = 0.1$ eV and $J'_{\text{ex}} = 0.4$ eV for Ni and $J_{\text{ex}} = J'_{\text{ex}} = 1.78$ eV for Fe. Due to the higher symmetry in fcc or bcc bulk crystals, only one crystal field parameter Δ_{Fe}^V (Δ_{Ni}^V) appears in the corresponding Fe (Ni) bulk Hamiltonian. For the monolayer, one would have to consider three different Δ 's because of the reduced symmetry, but these parameters are not known. Hence, only $\Delta_{\text{Fe/Ni}}^V$ has been considered in Eq. (2). The influence of further crystal field effects on E_{anis} in the monolayer, which was stressed by Bruno,¹⁰ is investigated in Sec. III C.

For a quantitative comparison with experiment, however, $4s$ states have to be included (within the so-called ‘‘combined interpolation scheme’’²¹) due to the strong overlap and hybridization between $3d$ and $4s$ bands in $3d$ transition metals. According to the pseudopotential method by Harrison,³⁰ the $4s$ electrons are described by a set of plane waves

$$\psi_{\mathbf{K}_j\mathbf{k}}(\mathbf{r}) = \frac{1}{\sqrt{N_U}} e^{i(\mathbf{k} - \mathbf{K}_j) \cdot \mathbf{r}},$$

where the \mathbf{K}_j are a set of reciprocal lattice vectors. They have to be chosen such that at least the lowest eigenstates in the considered part of the two dimensional Brillouin zone (irreducible part, see below) are described. For simple quadratic monolayers, this yields $\mathbf{K}_1 = (0, 0)$, $\mathbf{K}_2 = 2\pi/a(1, 0)$, $\mathbf{K}_3 = 2\pi/a(0, 1)$, $\mathbf{K}_4 = 2\pi/a(1, 1)$, $\mathbf{K}_5 = 2\pi/a(-1, 0)$, and $\mathbf{K}_6 = 2\pi/a(1, -1)$. To maintain the symmetry of the problem (and thus the correct occurrence of band degeneracies

TABLE I. Band structure parameters within the combined interpolation scheme for Fe and Ni (001) monolayers with lattice constant a . The parameters \bar{B}_i and Δ^V are taken from Pustogowa *et al.* (Refs. 28 and 29) for Fe and from Weling and Callaway (Refs. 26 and 27) for Ni (bulk parameters). The other parameters are obtained from a fit to *ab initio* calculations for freestanding (001) monolayers by Pustogowa *et al.* (Ref. 31) for Fe and Jepsen *et al.* (Ref. 32) for Ni.

	Fe	Ni
\bar{B}_1 (eV)	0.077 4	0.152 923
\bar{B}_2 (eV)	-0.008 16	-0.015 135
\bar{B}_3 (eV)	0.077 4	0.227 635
\bar{B}_4 (eV)	-0.153 24	-0.25
\bar{B}_5 (eV)	-0.056 52	-0.071 149
\bar{B}_6 (eV)	0.083 76	0.119 380
Δ^V (eV)	0.068	0.059 360
S^\uparrow	2.06	1.33
S^\downarrow	2.63	1.52
J_{ex} (eV)	2.18	0.87
J'_{ex} (eV)	2.18	1.17
E_0 (eV)	-0.54	-0.935
α (eV)	20.0	25.2
V_{00} (eV)	-4.20	-4.60
V_{10} (eV)	1.2	0.4
V_{11} (eV)	1.0	2.0
B_1 (eV)	7.5	5.0
B_2 (eV)	5.1	12.8
a (Å)	2.76	2.49

that turn out to be very important for E_{anis}), *symmetry factors* F_i have to be introduced into the Hamilton matrix.²¹ This leads to

$$H_{ij}^s = \langle \psi_{\mathbf{K}_i, \mathbf{k}} | H | \psi_{\mathbf{K}_j, \mathbf{k}} \rangle = \begin{cases} V_{00} + \alpha(\mathbf{k} - \mathbf{K}_i)^2 & \text{for } i=j, \\ V_{\mathbf{K}_j - \mathbf{K}_i} F_i F_j & \text{else.} \end{cases}$$

V_{00} , V_{10} , V_{11} , V_{12} , and V_{02} are the Fourier components of the pseudopotential, α is the dispersion of the 4s band. The symmetry factors are

$$F_1 = 1, \quad F_2 = \sin 2\xi, \quad F_3 = \begin{cases} \sin 2\eta & \text{for } \eta \geq 0, \\ 0 & \text{else,} \end{cases}$$

$$F_4 = F_2 F_3, \quad F_5 = \begin{cases} \sin 2\eta & \text{for } \eta \leq 0, \\ 0 & \text{else,} \end{cases} \quad F_6 = F_2 F_5.$$

The s - d hybridization H^{sd} between states of parallel spins is calculated according to Hodges *et al.*²¹ with the parameters B_1 and B_2 . To obtain accurate parameters, we perform a fit to the full-potential linear muffin-tin orbitals (LMTO) calculation for a free-standing Fe monolayer by Pustogowa *et al.*³¹ and to the linear augmented plane wave (LAPW) calculation for a Ni monolayer by Jepsen *et al.*³² The resulting param-

eters are listed in Table I. In order to reduce the number of free parameters in the fit, the d -band parameters \bar{B}_i and Δ^V are still taken from the corresponding bulk crystals (see above). To obtain correct d -band widths, however, the \bar{B}_i are scaled with the fitted parameters S^\uparrow and S^\downarrow for the spin-up and spin-down bands, respectively. Finally, the s - and d -band widths and s - d -hybridization parameters are scaled with t according to Harrison³³ to take into account the Cu surface lattice constant a :

$$\left(\frac{a}{a_0} \right)^q = \left(\frac{t}{t_0} \right) \quad (3)$$

with a_0 the surface lattice constant of Fe or Ni, t_0 the corresponding hopping parameters, and q being -5 for the dd parameters, -2 for the ss parameters, and $-7/2$ for the sd parameters. The in-plane lattice constant is taken to be that of the Cu substrate for all considered systems ($a = 2.56$ Å). This is correct for Ni, which is known to have a large pseudomorphic growth range.²² For Fe, however, both an in-plane nearest-neighbor distance similar to that of Cu and a smaller one³⁴ have been reported.

B. Spin-orbit coupling

Spin-orbit coupling (SOC) between the d states, leading to magnetocrystalline anisotropy, is introduced in the usual form as $H_{\text{so}} = \lambda_{\text{so}} \mathbf{l} \cdot \mathbf{s}$. It can be expressed⁸ by the components of the orbital momentum operator \mathbf{l} in the rotated frame (x_M, y_M, z_M) . Here, z_M is the spin quantization axis, which is parallel to the direction of magnetization (θ, ϕ) .³⁵

$$H_{\text{so}} = : \begin{pmatrix} H_{\text{so}}^{\uparrow\uparrow} & H_{\text{so}}^{\uparrow\downarrow} \\ H_{\text{so}}^{\downarrow\uparrow} & H_{\text{so}}^{\downarrow\downarrow} \end{pmatrix} = \frac{\lambda_{\text{so}}}{2} \begin{pmatrix} l_{z_M} & l_{x_M} - i l_{y_M} \\ l_{x_M} + i l_{y_M} & -l_{z_M} \end{pmatrix}. \quad (4)$$

Expressed in the basis of Eq. (1), H_{so} is a matrix function of the magnetization direction (θ, ϕ) . The SOC constant λ_{so} is taken from the corresponding atom: $\lambda_{\text{so}} = 70$ meV for Ni and 50 meV for Fe.³⁶

Unlike in usual tight-binding calculations,^{7,8,10,14} SOC is included nonperturbatively³⁷ in our treatment. Thus, we obtain important information on how E_{anis} scales with the SOC constant λ_{so} , which contributes to our analysis of the origin of E_{anis} in terms of band structure properties (see below).

C. Multilayers

We build up the Hamiltonian of a system of l layers by coupling l monolayer Hamiltonians $H_{\text{mono}}^{i=1 \dots l}$ together. The coupling of the layers is described within the tight-binding nearest-neighbor formalism used for the monolayer. Because of the missing periodicity in the z direction, we obtain terms that depend only on ξ and η . For the sake of simplicity, we take only σ bonds into account and obtain the following terms for the coupling of the orbital j of the monolayer i with the orbital k of the monolayer $i+1$, $H_{j,k}^{i,i+1}$:

$$H_{22}^{i,i+1} = -2\bar{B}_1 \cos 2\eta,$$

$$H_{33}^{i,i+1} = -2\bar{B}_1 \cos 2\xi,$$

with $i=1 \cdots l-1$. The $(22l \times 22l)$ coupling matrix thus has only elements in the $(l-1)$ (22×22) blocks just above and below the diagonal. The parameter \tilde{B}_1 is the same as used for the monolayers, but it yet has to be scaled to the interlayer distance of the tetragonally distorted system, according to Eq. (3). We consider equidistant layers. For Ni, we take into account the reported compression of 3.2% to scale the interlayer hoppings.²² For Fe, we assume an expansion of about 5% as reported by Müller *et al.*¹⁸

D. Anisotropy energy

The magnetic anisotropy energy per atom is defined as

$$E_{\text{anis}}(n) := E_{\text{tot}}(\theta=0; n) - E_{\text{tot}}(\theta=\pi/2, \phi_0; n), \quad (5)$$

where $E_{\text{tot}}(\theta, \phi; n)$ is the ground-state energy per atom with a total of n $3d$ and $4s$ electrons per atom, and the magnetization direction³⁵ is denoted by (θ, ϕ) . The in-plane angle ϕ_0 is chosen such that the resulting $|E_{\text{anis}}|$ is the largest possible. At first, the anisotropic dipole-dipole interaction is neglected, since it hardly depends on the electronic structure. Nevertheless, it may be of the same order of magnitude as the magnetocrystalline anisotropy resulting from SOC and will thus be included later to obtain quantitative results. The total energy per atom E_{tot} (with the \mathbf{k} -space resolved energy $E_{\mathbf{k}}$) is given by

$$\begin{aligned} E_{\text{tot}}(\theta, \phi; n) &= \frac{1}{N} \sum_{\mathbf{k}} E_{\mathbf{k}}(\theta, \phi; n) \\ &= \frac{1}{N} \sum_{m, \mathbf{k}} E_{m\mathbf{k}}(\theta, \phi) f_0[E_{m\mathbf{k}}(\theta, \phi) - E_F(\theta, \phi; n)], \end{aligned} \quad (6)$$

with N the number of atoms. $f_0(\Delta E)$ is the Fermi function at zero temperature and $E_F(\theta, \phi; n)$ is the Fermi energy which, for a given band filling n , is determined self-consistently by

$$n = \frac{1}{N} \sum_{m, \mathbf{k}} f_0[E_{m\mathbf{k}}(\theta, \phi) - E_F(\theta, \phi; n)].$$

$E_{m\mathbf{k}}(\theta, \phi)$ is the m th eigenvalue with crystal momentum \mathbf{k} and magnetization along (θ, ϕ) of the Hamiltonian

$$H_{\text{mono}} = H^d + H_{\text{so}}$$

for the monolayer in the tight-binding scheme and

$$H_{\text{mono}} = H^s + H^d + H^{sd} + H_{\text{so}}$$

for the monolayer in the combined interpolation scheme. For multilayer systems, we have the following Hamiltonian:

$$H = H_{\text{mono}}^1 \oplus \cdots \oplus H_{\text{mono}}^n + H_{\text{coupling}}.$$

In Eq. (6), we use the so-called *force theorem*, the validity of which has been assumed in all calculations of the magnetocrystalline anisotropy so far.

The complete Brillouin zone (BZ) summation over \mathbf{k} is performed as a weighted summation over the irreducible part of the BZ (for an arbitrary direction of magnetization). For the d electrons with SOC, that means a summation over 1/4 of the BZ. About 2000 points of the 1/4 BZ are then sufficient to achieve convergence. Note that we do not have to

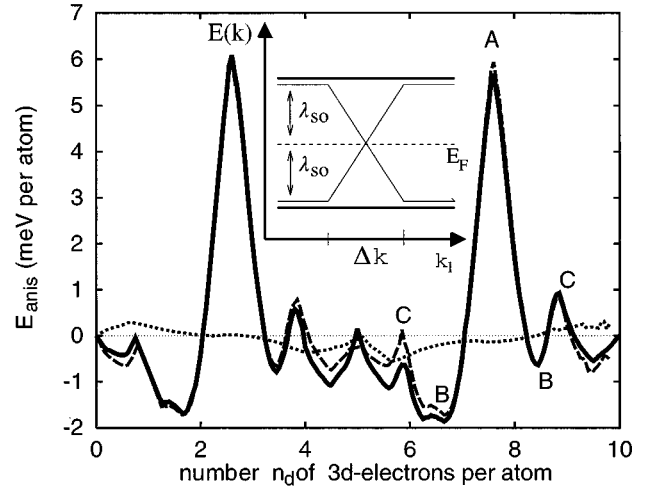


FIG. 1. Dependence of the magnetocrystalline anisotropy energy E_{anis} on the $3d$ -band filling n_d for a monolayer with parameters referring to Fe, calculated within the tight-binding scheme (solid curve). Negative values of E_{anis} yield perpendicular anisotropy. The origin of the peaks denoted by A, B, and C can be traced back to degeneracies in the band structure (see text, Fig. 3, and inset). The dashed and dotted curves show the contributions $E_{\text{anis}}^{\text{par}}$ and $E_{\text{anis}}^{\text{antipar}}$ to E_{anis} from the spin-orbit coupling between parallel spins and antiparallel spins, respectively. Inset: Occurrence (thin line) and lifting (thick line) of a ‘line’ degeneracy for two different directions of magnetization, z_M^x and z_M^y , respectively. \mathbf{k}_1 corresponds to one particular direction in \mathbf{k} space. Perpendicular to \mathbf{k}_1 , the intersecting bands are nondispersive throughout the BZ. The energy gained by the lifting of this degeneracy is given by $\Delta E_{\text{anis}} = \frac{1}{2} \lambda_{\text{so}} F$, if E_F falls in between the two subbands (dotted line). Here, F is the fraction of the involved states in \mathbf{k} space. If E_F lies below or above the two subbands, ΔE_{anis} is zero.

exclude any parts of the BZ to obtain convergence, unlike Wang *et al.*¹² Adding s electrons and s - d hybridization implies a coupling of non-SOC-coupled states with the SOC-coupled d states and results in a reduced symmetry. It is then necessary to perform the summation over 1/2 of the BZ. We then need 150 000 points to obtain the correct fourfold symmetry of the in-plane anisotropy energy as a function of the magnetization direction in the plane ($\cos 4\phi$). Fortunately, the out-of-plane anisotropy energy E_{anis} as defined by Eq. (5), which is larger by two orders of magnitude in our calculation ($E_{\text{anis}}^{\text{in-plane}} \simeq 1.2 \mu\text{eV}$ for Fe)³⁸ already converges for about 7000 points, so that calculations for systems of up to 14 layers are feasible.

III. RESULTS AND DISCUSSION

A. Monolayers within the tight-binding scheme

In Figs. 1 and 2, results for E_{anis} as a function of the $3d$ -band filling n_d are presented (solid lines) for the parameters of Fe and Ni monolayers, respectively. We use the lattice constant of 2.56 Å to simulate epitaxial growth on Cu(001). These figures demonstrate the correspondence between electronic structure and magnetic anisotropy and show that our method will yield convergent results for the whole transition metal series and for large (Fe) and small (Ni) ex-

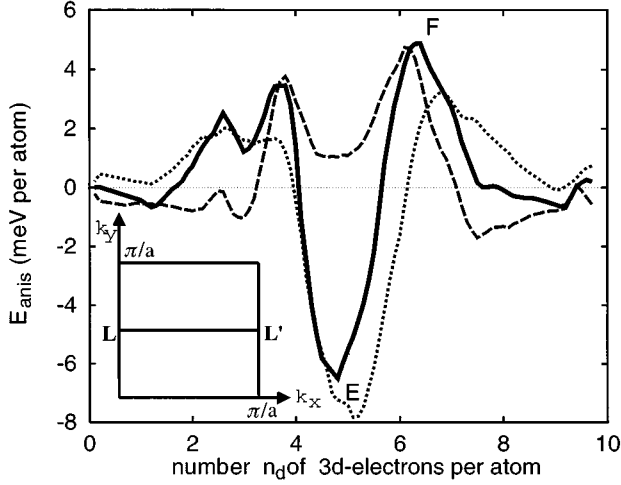


FIG. 2. Dependence of the magnetocrystalline anisotropy energy E_{anis} on the 3d-band filling n_d for a monolayer with parameters referring to Ni, calculated within the tight-binding scheme (solid curve). Negative values of E_{anis} yield perpendicular anisotropy. The origin of the peaks denoted by E and F can be traced back to degeneracies in the band structure (see text). The dashed and dotted curves show the contributions $E_{\text{anis}}^{\text{par}}$ and $E_{\text{anis}}^{\text{antipar}}$ to E_{anis} from the spin-orbit coupling between parallel spins and antiparallel spins, respectively. Inset: Irreducible part of the two-dimensional Brillouin zone of Fe for the tight-binding scheme. a is the lattice constant of the monolayer. The main contribution to E_{anis} at $n=8.8$ (corresponding to $n_d=7.6$ in the tight-binding calculation) results from the lifting of degeneracies along the line LL' .

change coupling. They will be analyzed in the following. Yet, the numerical value of E_{anis} for Fe and Ni monolayers cannot be extracted from these figures until the 4s electrons are included (see Sec. III C), since the exact 3d-band filling of the monolayers is not known.

Splitting the spin-orbit coupling matrix H_{so} into two parts, one of them ($H_{\text{so}}^{\text{par}}$) containing only coupling between states of parallel spin, the other one ($H_{\text{so}}^{\text{antipar}}$) between states of opposite spin, and recalculating E_{anis} as a function of n_d with either of the two matrices instead of H_{so} itself, we obtain the curves $E_{\text{anis}}^{\text{par}}(n_d)$ and $E_{\text{anis}}^{\text{antipar}}(n_d)$, respectively (Figs. 1 and 2, dashed and dotted lines, respectively). Note that to a good approximation $E_{\text{anis}}^{\text{par}}(n_d) + E_{\text{anis}}^{\text{antipar}}(n_d) \approx E_{\text{anis}}(n_d)$ is valid. For Fe parameters, $E_{\text{anis}}^{\text{antipar}}(n_d)$ is very small due to the large exchange splitting J_{ex} that completely separates the spin subbands. Thus, $E_{\text{anis}}^{\text{antipar}}(n_d)$ is ineffective and may therefore be neglected for further analysis. The curve $E_{\text{anis}}^{\text{par}}(n_d) \approx E_{\text{anis}}(n_d)$ consists of two parts of equal shape, viz., for $n_d \in [0; 5]$ (spin-up band) and $n_d \in [5; 10]$ (spin-down band). In the case of Ni, $E_{\text{anis}}^{\text{par}}(n_d)$ and $E_{\text{anis}}^{\text{antipar}}(n_d)$ are of the same order of magnitude, since there is a considerable overlap between the spin-up and spin-down subbands.

The curves $E_{\text{anis}}(n_d)$ show a number of pronounced peaks (A, B, C, E, F in Figs. 1 and 2), the origin of which has to be clarified. Two possible contributions to E_{anis} are discussed in the literature.^{11–13} (i) The SOC-induced shifting of occupied, nondegenerate bands leads to contributions to E_{anis} in second-order perturbation theory with respect to the SOC

constant λ_{so} : $E_{\text{anis}} \propto \lambda_{\text{so}}^2$. The first order vanishes due to time reversal symmetry.¹⁰ (ii) The contribution of the lifting of degenerate bands, which are shifted linearly with λ_{so} , depends on the fraction of states in \mathbf{k} space influenced by the degeneracy. Whether this fraction is of the order of λ_{so}^2 , which would yield¹² $E_{\text{anis}} \propto \lambda_{\text{so}}^3$, or of lower order which would yield important contributions to E_{anis} ,^{11,13} has been a controversial question. Anyway, the scaling of E_{anis} with λ_{so} can present important information about the dominant contributions to E_{anis} . Thus, it is very useful not to restrict calculations to second-order perturbation theory as has been frequently done.^{10,14} Remarkably, we find $E_{\text{anis}}(n_d) \propto \lambda_{\text{so}}^2$ for most of the n_d values in agreement with Wang *et al.*¹² Unlike stated by those authors, however, this does not rule out contributions to E_{anis} of the lifting of degeneracies (ii). In Sec. III B and Fig. 1, we show explicitly that such contributions play a very important role for E_{anis} in the monolayers considered. This is true as well for the multilayers (see the discussion in Secs. III E and III F).

The dependence of E_{anis} on the scaling of all d -electron hopping parameters with a common parameter t was checked. We found that the overall shape of the curves $E_{\text{anis}}(n)$ will not change if t is varied. $|E_{\text{anis}}|$ increases for decreasing t (decreasing bandwidth). This leads to the general trend of $|E_{\text{anis}}|$ increasing with increasing lattice constant a of the monolayer, since t is proportional to a^{-5} (see Sec. III C).³³

B. The electronic origin of E_{anis}

In this chapter we discuss in detail how the magnetocrystalline anisotropy energy can be related to the electronic band structure. A 3d-band degeneracy can make large contributions to E_{anis} , if (i) it is lifted by SOC for one direction of magnetization (z_M^{Ξ}) and remains for another (z_M^X), (ii) it is located near the Fermi level E_F , (iii) it runs along a line in \mathbf{k} space, and (iv) the degenerate bands have no or very little dispersion along this line. Before showing that such degeneracies indeed occur in the band structures, we estimate their contribution within a linearized band structure (see inset of Fig. 1). If E_F is situated below or above the two subbands, no contribution to E_{anis} results, $\Delta E_{\text{anis}} = 0$. The maximal contribution occurs when the degeneracy lies exactly at the Fermi level E_F and amounts to

$$\Delta E_{\text{anis}} = \frac{\lambda_{\text{so}}}{2} F = \lambda_{\text{so}}^2 \left(\frac{\partial E}{\partial k_1} \frac{\pi}{a} \right)^{-1} \quad (7)$$

since the fraction F of involved states in the irreducible quarter of the BZ is $F = (\Delta k_1 / \pi/a)(\pi/a / \pi/a) = 2\lambda_{\text{so}} [(\partial E / \partial k_1)(\pi/a)]^{-1}$. The preferred direction of magnetization is z_M^{Ξ} .

Thus, ΔE_{anis} is proportional to λ_{so}^2 for a degeneracy that occurs along a *line* with the involved bands being nondispersive along that line. This agrees with the scaling of E_{anis} observed above. In their estimate of the contribution of degeneracies, Wang *et al.*¹² implicitly assume that the degenerate bands are dispersive in either dimension of \mathbf{k} space. This would lead to $F \propto \lambda_{\text{so}}^2$ and $E_{\text{anis}} \propto \lambda_{\text{so}}^3$ and justify the exclusion of degeneracies from their calculation in order to

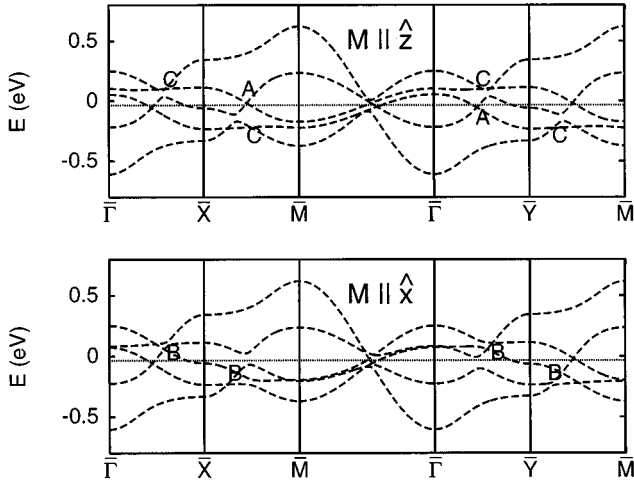


FIG. 3. Band structure of the 3d minority spin band of the Fe monolayer, calculated within the tight-binding scheme. The magnetization \mathbf{M} is directed along the layer normal \hat{z} (upper part) and in-plane along \hat{x} (lower part). The degeneracies denoted by A, B, and C contribute to the peaks A, B, and C in Fig. 1. The dotted lines denote the Fermi level for $n_d=7.6$, respectively. $\Gamma=(0,0)$, $\bar{X}=(\pi/a,0)$, $\bar{Y}=(0,\pi/a)$, and $\bar{M}=(\pi/a,\pi/a)$ are the high symmetry points of the irreducible part ($0 \leq k_x, k_y \leq \pi/a$) of the Brillouin zone. a is the lattice constant of the monolayer.

improve convergence. In the light of our results, however, this assumption is incorrect and it neglects very important contributions to E_{anis} .

In Fig. 3, some degeneracies are shown in the band structure of the Fe monolayer. For example, the degeneracy A that occurs for $\mathbf{M} \parallel \hat{z}$ and is lifted for $\mathbf{M} \parallel \hat{x}$ is located at the Fermi level for $n_d=7.6$ (dotted lines in Fig. 3) and leads to the peak A in Fig. 1. It runs along a line in \mathbf{k} space, which is shown in the inset of Fig. 2. According to Eq. (7), with $\partial E / \partial k_y = 0.6 \text{ eV} / \pi/a$ (taken from the band structure), this contribution should be $\Delta E_{\text{anis}} \approx 4 \text{ meV}$, which agrees in the order of magnitude with the calculated value $E_{\text{anis}}(n_d=7.6) = 6 \text{ eV}$.

Several tests have been made to support that hypothesis. Excluding the states influenced by the degeneracy A (4.3% of the total of 3d states) from the calculation of E_{anis} , the height of peak A is reduced to 40%. The \mathbf{k} -space resolved analysis of $E_{\text{anis}}(n_d=7.6)$ also shows clearly that E_{anis} results from the states near the degeneracy.

Analogous degeneracies are found in the Ni band structure contributing to the peaks E and F (Fig. 2). Note that the lifting of degeneracies can favor in-plane as well as perpendicular magnetization. This is in contradiction to the results of Daalderop *et al.* for a Co(111) monolayer,¹³ who state that degeneracies should always favor perpendicular magnetization.

Since the 3d-band degeneracies are so important for E_{anis} , we analyze in the following the occurrence and lifting of degeneracies in the band structure. It can be shown that, in terms of the basis of Eq. (1), the Hamilton matrix H^d [Eq. (2)] has the simplest block diagonal form with only four off-diagonal elements (ODE's) $H_{45}^d = H_{54}^d$ and, equivalently, $H_{9,10}^d = H_{10,9}^d$. To find out which additional ODE's are intro-

duced by SOC for a given direction of the magnetization \mathbf{M} , we analyze the form of H_{so} in Eq. (4). States with parallel spins are coupled if they contain equal orbital momenta with respect to the spin quantization axis z_M , whereas states with opposite spins must show a difference of one in the orbital momenta to yield nonvanishing ODE's. The real space components of the atomic states ϕ_i , $i=1, \dots, 5$, are composed of eigenstates of l_z with the eigenvalues $(-2,2)$, $(-1,1)$, $(-1,1)$, $(-2,2)$, and 0, respectively. In terms of eigenstates of l_x one has the eigenvalues $(-1,1)$, $(-2,2)$, $(-1,1)$, $(-2,0,2)$, and $(-2,0,2)$, respectively. This yields a coupling for $\mathbf{M} \parallel \hat{z}$ within the groups of states ψ_i with $i=1,4,5,7,8$ and with $i=2,3,6,9,10$, and, in the case of $\mathbf{M} \parallel \hat{x}$, within the groups of states ψ_i with $i=2,4,5,6,8$ and $i=1,3,7,9,10$, respectively. In both cases, the Hamiltonian can be split into two 5×5 blocks, and subbands belonging to different blocks will intersect. Between states of the same block, the degeneracies will usually be removed. Especially the subbands ψ_1 and ψ_2 (and, correspondingly, ψ_6 and ψ_7) change their roles if the magnetization is changed from \hat{z} to \hat{x} and vice versa, because the orbitals xy and yz have different orbital momenta with respect to the x and z axes. These subbands will thus be involved in the lifting of degeneracies by altering magnetization and possibly, as shown above, yield important contributions to E_{anis} . In the case of Fe parameters, the situation is even simpler since coupling between states of opposite spin (ψ_i and ψ_j with $i \leq 5 < j$) can be neglected.

As an example, peak A in the curve $E_{\text{anis}}(n)$ of Fe at $n=7.6$ (Fig. 1) results from the degeneracy A (Fig. 3) of the subbands corresponding to the states ψ_7 and (ψ_9, ψ_{10}) . Thus, it occurs for $\mathbf{M} \parallel \hat{z}$, and is lifted for $\mathbf{M} \parallel \hat{x}$, since in the second case the subbands belong to the same block of the Hamiltonian, whereas in the first they do not.

As a conclusion, it has been shown that 3d-band degeneracies along lines of constant energy result in important contributions to E_{anis} if they occur near the Fermi level. They can favor in-plane and perpendicular magnetization and need not occur near high symmetry points of the BZ. Thus, for (001) layers, it is not sufficient to consider only bands at high symmetry points as was done by Daalderop *et al.*¹³ for a Co(111) monolayer. Furthermore, for such contributions from degeneracies, $E_{\text{anis}} \propto \lambda_{\text{so}}^2$ and, approximately, $E_{\text{anis}} \propto 1/\partial E / \partial k_1$ is valid (the band dispersion $\partial E / \partial k_1$ is approximately proportional to the scaling t of the hopping parameters) which agrees with the observations reported above. Note that the analysis is very simple due to the analytic form and low dimension of the 3d tight-binding matrix, which is an advantage of the semiempirical scheme. It remains valid if the extension to s states is performed (see below).

C. The results of the combined interpolation scheme

Results for $E_{\text{anis}}(n)$ obtained from the combined interpolation scheme (including s and d bands as well as s - d hybridization) for the monolayer are presented in Fig. 4 for Fe parameters and Fig. 5 for Ni parameters with the lattice constant of the Cu(001) surface in both cases (solid curves; the discussion of the curves for two and three layers is postponed to Secs. III E and III F). These results for the monolayer are similar to the curves for d bands only

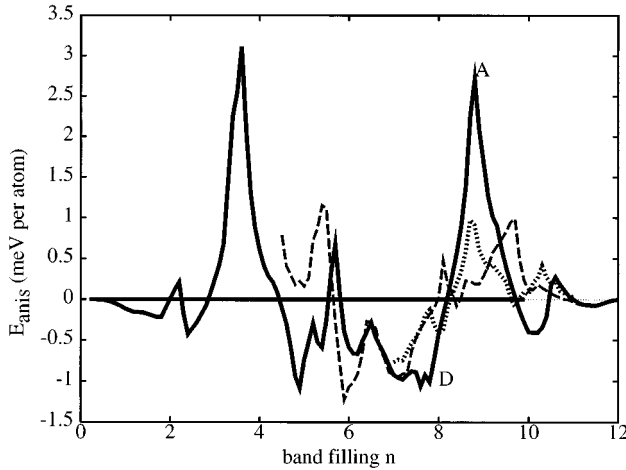


FIG. 4. Magnetic anisotropy energy of Fe as a function the s - and d -band filling for one layer (solid curve), two layers (dashed), and three layers (dotted). Peaks A and D are caused by the respective degeneracies in the band structure shown in Fig. 9.

(Figs. 1 and 2). n is the total filling of the s and d band ($n=8$ for Fe and $n=10$ for Ni). We find for a Fe monolayer $E_{\text{anis}}(\text{Fe/Cu}) = -0.41$ meV per atom and for Ni, $E_{\text{anis}}(\text{Ni/Cu}) = 0.10$ meV per atom. The dipole-dipole interaction is included under the assumption of a point dipole located at each site, carrying the magnetic moment of the unit cell. The (spin) magnetic moment per atom is calculated from the band structure [$m(\text{Fe/Cu}) = 3.3\mu_B$ and $m(\text{Ni/Cu}) = 0.91\mu_B$]. The dipole anisotropy (equivalent to the shape anisotropy in the monolayer) always prefers in-plane magnetization. Altogether, we obtain for the total magnetic anisotropy energy per atom of a Fe and Ni monolayer with the lattice constant of Cu(001)

$$E_{\text{anis}}^{\text{tot}}(\text{Fe/Cu}) = -0.17 \text{ meV}$$

and

$$E_{\text{anis}}^{\text{tot}}(\text{Ni/Cu}) = 0.12 \text{ meV}$$

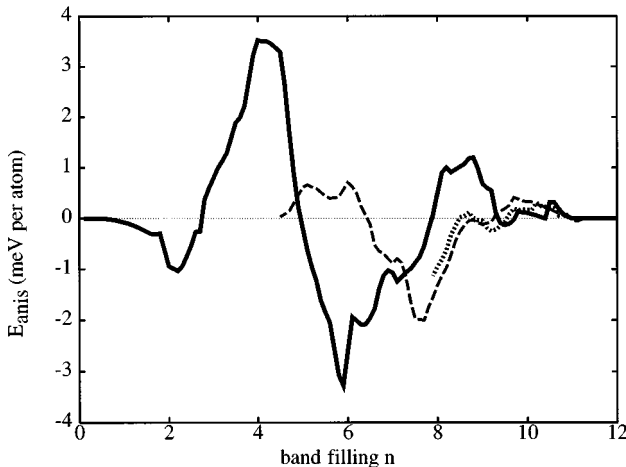


FIG. 5. Magnetic anisotropy energy of Ni as a function the s - and d -band filling for one layer (solid curve), two layers (dashed), and three layers (dotted).

with the easy axis perpendicular to the monolayer for Fe and in-plane for Ni. Note that corresponding *ab initio* results for a free-standing Fe-monolayer yielded -0.42 meV,^{9,12} but previous tight-binding calculations gave the too large value of -5.5 meV.¹⁴

In the case of Fe, the perpendicular easy axis of ultrathin Fe films on Cu(001) is reproduced correctly. Direct comparison with a Fe monolayer on Cu(001) is difficult due to film growth problems.⁴ It is common to separate the anisotropy energy of thin films into a volume and a surface term:^{5,22}

$$E_{\text{anis}}(d) = \mathbf{K}_v + \frac{2\mathbf{K}_s}{d}, \quad (8)$$

The first term, \mathbf{K}_v , describes the thickness-independent contributions to the anisotropy energy and the second, \mathbf{K}_s , the thickness-dependent contributions and the surface effects. Fowler and Barth measured the following anisotropy constants:⁵ $\mathbf{K}_v = 0.132$ meV/atom and $\mathbf{K}_s = 0.11$ meV/atom for the distorted fcc films at 100 K. The value $\mathbf{K}_v + 2\mathbf{K}_s = 0.352$ meV/atom is comparable to our result. This result has been calculated with the measured anisotropy field using the bulk saturation magnetization of bcc Fe. For Ni, our result also agrees very well with experiments²² which yields $E_{\text{anis}}(\text{Ni/Cu}) = 0.125$ meV at 300 K. The anisotropy constants \mathbf{K}_s and \mathbf{K}_v are temperature dependent. Measurements of the anisotropy constants as a function of the reduced temperature have been made,³⁹ but the correct extrapolation to $T=0$ K is not known yet. While in experiment, the values of K_v and K_s have to be compared at the same reduced temperature because of the thickness dependence of T_c , the theoretical values are for 0 K and thus independent of the difference of absolute and reduced temperature.

Note that in Fig. 5, the curve $E_{\text{anis}}(n)$ for the Ni monolayer (solid curve) has zeros near $n=10$. Hence, the numerical result for Ni is not very stable and the excellent agreement with experiment should not be overemphasized. Nevertheless, for Fe and Ni, the sign and the order of magnitude of E_{anis} turn out to be remarkably stable upon parameter variations: Sign changes do not occur upon variation of the pseudopotential and s - d hybridization parameters by as much as 40%. Moreover, we find in agreement with Wang *et al.*¹² a perpendicular easy axis also for Fe monolayers taking (001) surface lattice constants imposed by substrates such as Pd, Ag, and V (2.77, 2.89, and 3.03 Å), respectively. This stability again demonstrates the validity of our results for E_{anis} . The good agreement of the results both with *ab initio* theories and experiments is due to the fact that the parameters were obtained by a fit to *ab initio* calculations for Fe and Ni monolayers rather than taking bulk parameters.

To investigate crystal field effects, an additional parameter Δ is introduced¹⁰ to take into account the different effect of the monolayer geometry on orbitals that lie in the plane of the monolayer (xy and $x^2 - y^2$) and out-of-plane orbitals (yz , zx , and $3z^2 - r^2$). In addition to Eq. (2), the on-site energies of the latter are lowered by Δ with respect to the former. The dependence of E_{anis} on Δ is shown in Fig. 6 for Fe and Ni parameters (solid and dashed curve, respectively). Remarkably, $\Delta = 0.2$ eV changes the sign of E_{anis} for both systems considered. Thus, it is important to determine Δ from the *ab initio* band structures. In the case of Fe, the fit of

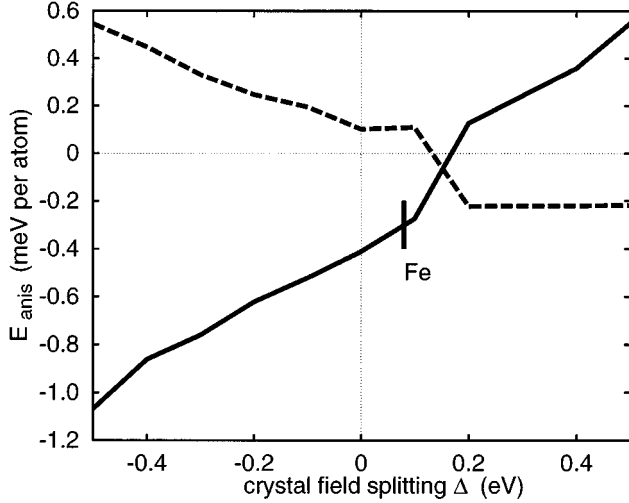


FIG. 6. Dependence of the magnetocrystalline anisotropy energy E_{anis} on the crystal field splitting Δ for the Fe monolayer on Cu(001), $n=8$ (solid curve) and the Ni monolayer on Cu(001), $n=10$ (dashed curve). Negative values of E_{anis} yield perpendicular anisotropy. The vertical line denotes the best fit for Δ for the Fe monolayer. In the case of Ni, the fit cannot be improved by the introduction of Δ (see text).

the $3d$ bands near the Γ point of the BZ can be significantly improved by choosing $\Delta=0.08$ eV. The resulting $E_{\text{anis}}(\text{Fe/Cu})$ amounts to -0.30 meV, still with a perpendicular easy axis even if the dipole-dipole interaction is added. For Ni, the introduction of Δ does *not* improve the fit. Those results for Δ differ substantially from $\Delta=-0.5$ eV given by Bruno¹⁰ which has been determined by a fit to the Ni(111) monolayer but employed for both Fe and Ni(001) monolayers also. Pick and Dreysse¹¹ state that for (001) monolayers a crystal field parameter is not necessary. For Ni, this is supported by our result; even in Fe, our value of Δ is small compared to other band structure parameters. Cinal *et al.*¹⁴ report $\Delta=-0.14$ eV for the Ni(001) monolayer.

Finally, a detailed investigation of the band structures²⁵ shows that the analysis given in Sec. III B for $3d$ bands is still valid for the combined interpolation scheme. As evidence, consider Figs. 1 and 4 (solid curves): There is a one-to-one correspondence between the peaks in E_{anis} in both curves. This correspondence can be shown to result from similar band structure details. In particular, the role of $3d$ -band degeneracies stressed in Sec. III B remains the same in the complete scheme.

D. Temperature dependence

One of the greatest challenges in the investigation of magnetic anisotropy is the calculation of reorientation transitions with temperature. Up to now, a complete electronic and thermodynamic theory is lacking. Here, one-particle effects of temperature are investigated. It turns out that they again support the role of degeneracies for magnetic anisotropy and, moreover, are comparable in order of magnitude with the many-particle aspects usually considered.⁴⁰

The free magnetic anisotropy energy F_{anis} depends on temperature T due to (i) the Fermi distribution of electronic states $f_T(\Delta E)$, (ii) the hopping integrals, which depend on

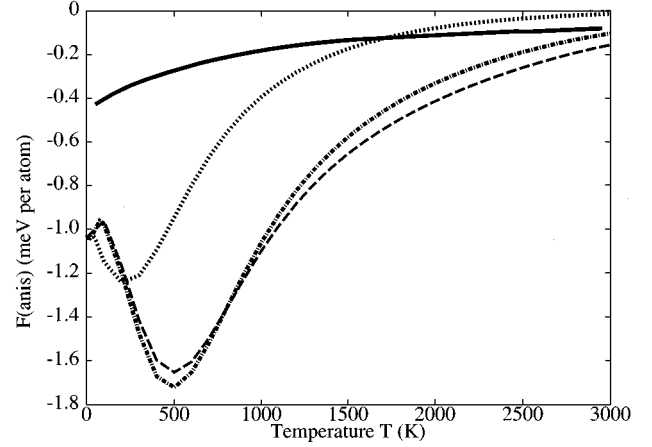


FIG. 7. Temperature dependence of $F_{\text{anis}}(T)$ for a Fe-parametrized d -band calculation for the monolayer with d -band filling $n_d=6$ (d -electrons only, dashed curves) and for three layers with band filling $n=8$ (s and d electrons, solid line). For the upper dashed curve, only Fermi statistics are taken into account, for the middle curve the lattice expansion is added, and the dotted curve includes the effects of Fermi statistics, lattice expansion, and entropy. The calculation for three layers includes Fermi statistics, lattice expansion, and entropy for s and d electrons.

T because of the lattice expansion of the substrate, (iii) the entropy $S(T)$, and (iv) the effects of spin-waves, resulting in a temperature dependence of the magnetization $\mathbf{M}(T)$. In this work, the first three effects are analyzed. More precisely, the thermal expansion (ii) of the lattice constant $a(T)$ is included by means of the empirical law $a(T)=a(T=0)(\alpha T+1)$. $\alpha=2 \times 10^{-5}/\text{K}$ is the expansion coefficient for the Cu substrate.⁴¹ The expression for the entropy (iii) of noninteracting particles is

$$S = -k_B \sum_{m,\mathbf{k}} \langle n_{m\mathbf{k}} \rangle \ln \langle n_{m\mathbf{k}} \rangle + (1 - \langle n_{m\mathbf{k}} \rangle) \ln(1 - \langle n_{m\mathbf{k}} \rangle)$$

with $\langle n_{m\mathbf{k}} \rangle = f_T[E_{m\mathbf{k}}(\theta, \phi) - \mu(\theta, \phi; n)]$. In analogy to Eq. (5), the free magnetocrystalline anisotropy energy F_{anis} is defined as the difference in the free energy $F=E-TS$ for two different directions of magnetization.

Figure 7 shows $F_{\text{anis}}(T)$ (d -band calculation for the monolayer, Fe parameters, $n_d=6$). Including only Fermi statistics [(i) dashed curve], the characteristic energy scale for the decrease of $|F_{\text{anis}}|$ with T is about 1000 K (100 meV), which corresponds to the energy $2\lambda_{\text{so}}$, but not to the $3d$ -band width of approximately 3 eV. This becomes immediately plausible if one notices that the SOC-induced lifting of degeneracies occurs near the Fermi level. Thus, one expects a measurable effect on F_{anis} due to Fermi statistics as soon as $k_B T$ becomes larger than or comparable to $2\lambda_{\text{so}}$. In addition, we must conclude from our results that shifting of subbands far below the Fermi level is not so important, since then F_{anis} could not be essentially lowered on such a small temperature scale.

The characteristic increase of $|F_{\text{anis}}|$ with increasing temperature for $T < 500$ K is a direct result of the lifting of degeneracies. Consider again Fig. 1. For $\mathbf{M} \parallel \hat{z}_M^{\hat{z}}$ (lifted degen-

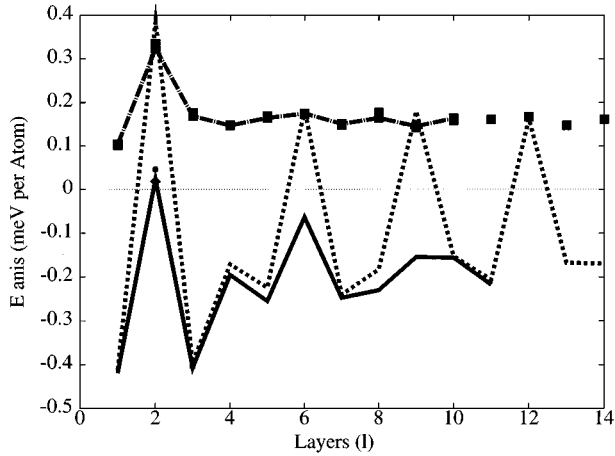


FIG. 8. Magnetic anisotropy energy of Fe and Nickel as a function of the number of layers calculated in the combined interpolation scheme. The calculation for 1/4 BZ for Fe (dashed line) yields periodic oscillations caused by the incorrect symmetry of $E_{\text{anis}}^{\text{in-plane}}$. Summation over 1/2 BZ (solid line) corrects this problem. For the Fe bilayer, the square and diamond are calculations with 15 356 and 108 228 points in the 1/2 BZ, respectively. For Nickel (broken line: 1/2 BZ, squares: 1/4 BZ), the convergence is better.

eracy), which is the energetically favored case, Fermi statistics induces only little changes in the occupation of the electronic states, if $k_B T < \lambda_{so}$; for the degenerate bands ($\mathbf{M} \parallel z_M^X$), however, states in the upper band are significantly occupied even for $k_B T < \lambda_{so}$. Thus, the total energy for $\mathbf{M} \parallel z_M^X$ rises with respect to $T=0$ in this temperature range. This leads to an increase of $|F_{\text{anis}}|$ with increasing T , if $k_B T < \lambda_{so} = 50$ meV ($T < 500$ K).

The inclusion of lattice expansion [(ii) solid curve in Fig. 7] has only a small effect on F_{anis} . The narrowing of bands with increasing temperature due to the scaling of the hoppings leads to an increase in $|F_{\text{anis}}|$ for small T , which was already discussed for $T=0$. For larger T , the influence of Fermi statistics on narrowed bands is larger, leading to a stronger decrease of $|F_{\text{anis}}|$.

The entropy [(iii) dotted curve] has a damping effect on the curve $F_{\text{anis}}(T)$, but maintains the features discussed above. This results from the fact that, in the case of degenerate bands, the entropy is larger than for nondegenerate bands, since states located nearer to the Fermi level have larger entropy.

$F_{\text{anis}}(T)$ was also calculated for three layers within the combined interpolation scheme (Fig. 7), taking into account all three mentioned effects and shows a decrease with increasing temperature on the same scale as for the monolayer. Hence, this analysis of $F_{\text{anis}}(T)$ shows the significant contribution of temperature-induced changes of the degeneracies to the anisotropy energy. It is remarkable that the three temperature effects mentioned above, and particularly the electron temperature dependence of the Fermi function, are of equal magnitude as the temperature effects of spin waves on $\mathbf{M}(T)$.

E. Fe Multilayers

Figure 8 shows the calculated magnetic anisotropy energy

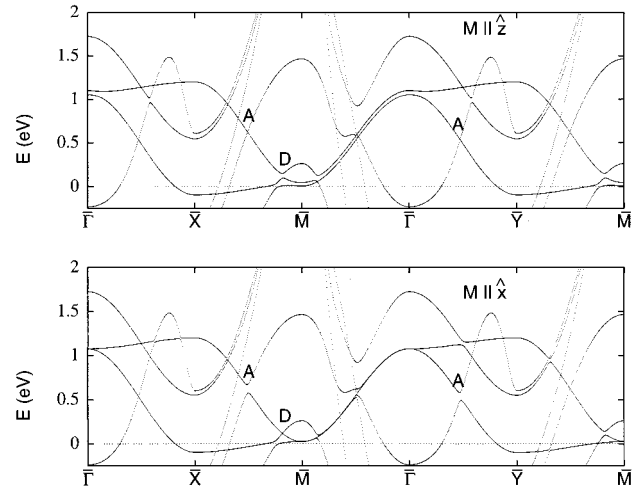


FIG. 9. Monolayer band structure of the 3s and 4s band for Fe parameters, calculated within the combined interpolation scheme with the magnetization \mathbf{M} parallel to the layer normal z in the upper part and in-plane parallel x in the lower part. High symmetry points are the same as in Fig. 3.

for Fe films of 1 to 14 layers. Calculations for both 1/4 BZ and 1/2 BZ are included. The values obtained when the summation over \mathbf{k} is performed over 1/4 BZ lead to periodically recurring positive values of E_{anis} (for films of 2, 6, 9, and 12 layers). The positive value for a film thickness of 2 layers can be traced back to the occurrence of degeneracy A at the Fermi level. For the other positive values, the easy and hard axes are found to be in-plane, an effect of the wrong symmetry resulting from the summation over 1/4 BZ, leading to an overestimation of the *in-plane* anisotropy $E_{\text{anis}}^{\text{in-plane}}$. We perform the \mathbf{k} -space summation again, this time over 1/2 BZ, thus respecting the symmetry of the *s-d* hybridized system. This reduces the importance of degeneracy A and we find positive values only at 2 and 6 ML. It turns out that a new degeneracy D is responsible for the negative values. In order to demonstrate this relationship between the easy axis and the band structure for the multilayer systems, we go back to the monolayer at a slightly different band filling. The degeneracy A observed for the monolayer in the tight-binding scheme is easy to recognize in Fig. 9, and a new degeneracy D is found near the M point for $\mathbf{M} \parallel \hat{x}$. Degeneracy D is lifted for $\mathbf{M} \parallel \hat{z}$, thus leading to a negative anisotropy energy. The \mathbf{k} -space analysis of the anisotropy energy confirms the importance of degeneracy D, which causes the ring-shaped dip around M . The structure seen along the line LL' (see the inset of Fig. 2) is the onset of the positive peak in the anisotropy energy caused by degeneracy A (see Fig. 4). Summation of the contributions of the \mathbf{k} points in the tenth of the BZ near M already gives half of the total anisotropy energy. Multilayer systems show per se more degeneracies than monolayers, and the contribution of these to the total anisotropy energy is not as clear as for the monolayer. Still, for a three layer system, we find again degeneracy D at the Fermi level, and recognize also in the \mathbf{k} space resolved anisotropy energy the characteristic structure it causes around M .

Taking Fig. 8 again and excluding the points of wrong symmetry (easy and hard axes in-plane) and the points where

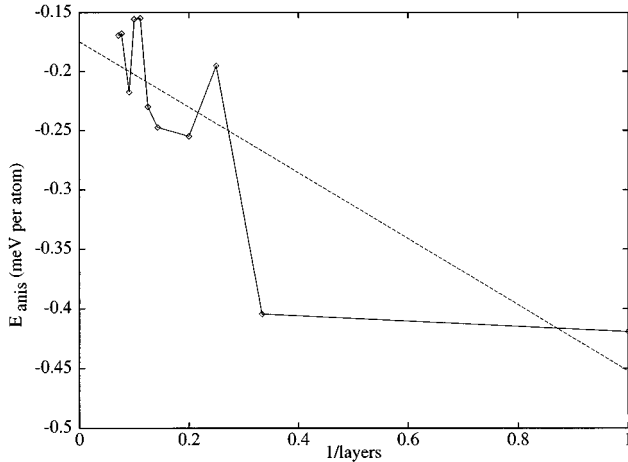


FIG. 10. Magnetic anisotropy energy of Fe as a function of the $1/l$ (l : number of layers). Including the dipole-dipole anisotropy energy, we obtain in-plane magnetization from the fourth layer on. A linear least square fit yields $\mathbf{K}_v = -0.17$ meV per atom and $\mathbf{K}_s = -0.14$ meV per atom.

we find degeneracy A at the Fermi level, we obtain the film thickness dependence of the magnetic anisotropy energy shown in Fig. 10. E_{anis} is plotted as a function of $1/l$. We expected a linear behavior [see Eq. (8)] and thus performed a linear least-square fit to the data. Although it is obvious that the calculated values do not exhibit the linear behavior very well, our fit yields $\mathbf{K}_v = -0.17$ meV per atom and $\mathbf{K}_s = -0.14$ meV per atom, which is in very good agreement with Fowler and Barth.⁵

Including the dipole-dipole anisotropy energy as calculated by Szunyogh *et al.*,¹⁵ we find for Fe a change of the easy axis from perpendicular to in-plane at 4 ML [$E_{\text{anis}}^{\text{dip}}(4 \text{ layers}) = 0.59$ meV]. Our result indicates that the experimentally observed transition at 5 ML might be an intrinsic quality of fct films grown at low temperature. Szunyogh *et al.* calculated the anisotropy energy of thin fcc-Fe films on Au (001) and also observed oscillations and strong deviations from the expected linear behavior. They obtained a reorientation transition from perpendicular to in-plane magnetization at 4 ML.

In order to compare our calculated dependence of E_{anis} of Fe on the $3d$ - and $4s$ -band filling n with experiment, we go back to Fig. 4. For the monolayer at a s - and d -band filling of $n=8$, we are near a zero of the curve, and at $n=8.2$ we already have a positive value of E_{anis} caused by the growing influence of degeneracy A. We would thus expect a monolayer of a $\text{Fe}_x\text{Co}_{1-x}$ alloy to have an in-plane magnetization already at small Co concentrations. This was in fact measured by Dittschar *et al.*⁴² for $x=0.95$. We would predict an increase of the anisotropy energy with increasing Co concentration. For three layers, we would expect the same behavior, the structure of the curve $E_{\text{anis}}(n)$ near $n=8$ being similar to that of the monolayer. This alloying behavior found both theoretically and experimentally supports the relevance of degeneracies for the anisotropy energy, as claimed by Daalderop *et al.* and disputed by Wang, Wu, and Freeman. In the case of $\text{Fe}_x\text{Co}_{1-x}$, there is no doubt that the magnetic moment persists.

F. Ni multilayers

In this paragraph, we discuss the thickness dependence of the magnetic anisotropy energy of Ni and thus refer to the remaining curves of Figs. 5 and 8. The anisotropy for Ni bilayers and trilayers as a function of band filling is shown by the dashed and dotted curves in Fig. 5. Although the general shape of the curves closely resembles that of the monolayer, the peak positions and thus the direction of the easy axis at a given number of $4s$ and $3d$ electrons may differ. The magnetic anisotropy of Ni calculated for systems of 1 to 14 ML is shown in Fig. 8. We include again calculations using $1/4$ of the BZ and $1/2$ BZ, but this time no point has to be excluded. E_{anis} of the second layer is much bigger than that of the monolayer, a fact which perhaps indicates that the influence of the substrate cannot be neglected. The anisotropy then drops again and remains approximately constant at a value of about 0.14 meV (which is still bigger than the value obtained for the monolayer). Schulz and Baberschke²² report for Ni a transition from in-plane to perpendicular magnetization at 7 ML, due to a large \mathbf{K}_v which favors a perpendicular orientation of the magnetization. Our theory does not reproduce this reorientation.

For Fe, the behavior of the films as a function of thickness could be related to the degeneracies occurring at the Fermi level. The contribution of these degeneracies to the total anisotropy of the film would be expected to decrease with increasing number of layers, as their weight in the summation over all atoms (number of points in the BZ \times number of layers) decreases: that is in fact what we find for Fe. For Ni, however, the contribution of the degeneracies to the anisotropy energy is not so evident. The minority and majority spin bands mix much more than in the case of Fe because of the small exchange coupling. This is a possible reason for the nearly constant anisotropy energy we obtain. The occurrence of a degeneracy of a l -times degenerated band would also probably lead to a thickness independent contribution to E_{anis} .

So far, no other monolayer calculation lead to the correct in-plane anisotropy for the Ni monolayer. In a calculation for the fct bulk, Eriksson⁴³ finds a perpendicular easy axis, which is correct for fct Ni. Upon varying the c/a ratio in their calculation, however, these authors are unable to obtain in the limit of fcc Ni ($c/a = 1$) the correct easy axis, which is along the (111) direction. The same problem occurred in a previous total energy calculation of the same group for fcc Ni.⁴⁴ This seems to be a general problem of all calculations. We obtain the correct in-plane anisotropy for the monolayer, but the wrong \mathbf{K}_v . So, a three-dimensional calculation for fct Ni and variable c/a ratio also does not really tackle the problem of fcc Ni and cannot explain the behavior of the magnetization.

Ni is a delicate system. Maybe many-body effects cannot be neglected (i.e., the *force theorem* does not work well). The dependence between the anisotropy energy and the band structure seem to be very subtle and the smallest details can influence the results.^{45,46}

IV. CONCLUSIONS

A calculation of the magnetocrystalline anisotropy energy E_{anis} of Fe and Ni monolayers on Cu(001) is performed. In agreement with experiments, we find a perpendicular easy

axis for Fe and an in-plane easy axis for Ni. The results are fully converged without any additional assumption to improve convergence. SOC is included nonperturbatively. It is an important result that large contributions to E_{anis} can result from the SOC-induced lifting of degeneracies occurring along *lines* in \mathbf{k} space at the Fermi level. The contributions of those degeneracies scale with the square of the SOC constant λ_{so} , as contributions from nondegenerate bands do. The occurrence and lifting of degeneracies in the $3d$ band has been discussed in general. Evidence for the important contribution to E_{anis} of the degeneracies at the Fermi-level are (i) the groove and the ring-shaped dip in the \mathbf{k} space resolved anisotropy for the monolayer in the tight-binding scheme, and

in the combined interpolation scheme respectively, (ii) the temperature dependence (the characteristic energy scale for the decrease of the free magnetocrystalline anisotropy energy $|F_{\text{anis}}|$ as a function of the temperature is determined by λ_{so}), (iii) the finite anisotropy energy at T_c , and (iv) the alloying behavior of $\text{Fe}_x\text{Co}_{1-x}$. We obtain for Fe a reorientation transition from perpendicular to in-plane magnetization at 4 ML, which is independent of any restructuring of the fct film. Since it can be seen from Figs. 4 and 5 that both Fe and Ni do not exhaust the maximal anisotropy possible, our calculation of E_{anis} should also be important for the technologically relevant maximization of magnetic anisotropy by appropriate surface-alloy formation.

- ¹J. H. Van Vleck, Phys. Rev. **52**, 1178 (1937).
²M. L. Néel, J. Phys. Radium **15**, 225 (1954).
³R. Druzinic and W. Hübner, Phys. Rev. B **55**, 347 (1997).
⁴D. P. Pappas, K.-P. Kämper, and H. Hopster, Phys. Rev. Lett. **64**, 3179 (1990); J. Thomassen *et al.*, **69**, 3831 (1992).
⁵D. E. Fowler and J. V. Barth, Phys. Rev. B **53**, 5563 (1996).
⁶D. Li *et al.*, Phys. Rev. Lett. **72**, 3112 (1994).
⁷A. J. Bennett and B. R. Cooper, Phys. Rev. B **3**, 1642 (1971).
⁸H. Takayama, K.-P. Bohnen, and P. Fulde, Phys. Rev. B **14**, 2287 (1976).
⁹J. G. Gay and R. Richter, Phys. Rev. Lett. **56**, 2728 (1986).
¹⁰P. Bruno, Phys. Rev. B **39**, 865 (1989).
¹¹Š. Pick and H. Dreysse, Phys. Rev. B **46**, 5802 (1992); **48**, 13 588 (1993); Š. Pick *et al.*, *ibid.* **50**, 993 (1994).
¹²Ding-sheng Wang, Ruqian Wu, and A. J. Freeman, Phys. Rev. Lett. **70**, 869 (1993); Phys. Rev. B **47**, 14 932 (1993); Phys. Rev. Lett. **71**, 2166 (1993).
¹³G. H. O. Daalderop, P. J. Kelly, and M. F. H. Schuurmans, Phys. Rev. Lett. **71**, 2165 (1993); Phys. Rev. B **41**, 11 319 (1990); **42**, 7270 (1990); **50**, 9989 (1994).
¹⁴M. Cinal, D. M. Edwards, and J. Mathon, Phys. Rev. B **50**, 3754 (1994).
¹⁵L. Szunyogh, B. Újfalussy, and P. Weinberger, Phys. Rev. B **51**, 9552 (1995).
¹⁶D. M. Bylander, Leonard Kleinman, Phys. Rev. B **52**, 1437 (1995); M. Weinert, R. E. Watson, and J. W. Davenport, *ibid.* **32**, 2115 (1985).
¹⁷J. V. Barth and D. E. Fowler, Phys. Rev. B **52**, 11 432 (1995).
¹⁸S. Müller *et al.*, Phys. Rev. Lett. **74**, 765 (1995).
¹⁹M. Zharnikov *et al.*, Phys. Rev. Lett. **76**, 4620 (1996).
²⁰J. Hunter Dunn, D. Arvanitis, and N. Martensson (unpublished).
²¹L. Hodges, H. Ehrenreich, and N. D. Lang, Phys. Rev. **152**, 505 (1966).
²²B. Schulz and K. Baberschke, Phys. Rev. B **50**, 13 467 (1994).
²³G. C. Fletcher, Proc. Phys. Soc. London **65**, 192 (1952).
²⁴J. C. Slater and G. F. Koster, Phys. Rev. **94**, 1498 (1954).
²⁵T. H. Moos, Master's thesis, Freie Universität Berlin, 1995.
²⁶F. Weling and J. Callaway, Phys. Rev. B **26**, 710 (1982).
²⁷The parameters A_i used by Weling and Callaway have to be transformed into the coordinate system used here by $\bar{B}_1=A_4$, $\bar{B}_2=A_2-A_3$, $\bar{B}_3=A_2+A_3$, $\bar{B}_4=-A_1$, $\bar{B}_5=-\frac{1}{3}(A_4+4A_5)$, $\bar{B}_6=(2/\sqrt{3})A_6$, and $J'_{\text{ex}}=J_{\text{ex}}(e_g)$, $J'_{\text{ex}}=J_{\text{ex}}(t_{2g})$.
²⁸U. Pustogowa, W. Hübner, and K. H. Bennemann, Phys. Rev. B **48**, 8607 (1993).
²⁹The corresponding transformation formulas are $\bar{B}_1=A_1$, $\bar{B}_2=A_2$, $\bar{B}_3=A_1$, $\bar{B}_4=(\frac{3}{4}A_4+\frac{1}{4}A_2)$, $\bar{B}_5=(\frac{1}{4}A_4+\frac{3}{4}A_2)$, $\bar{B}_6=(\sqrt{3}/4)(A_2-A_4)$, and $J'_{\text{ex}}=J_{\text{ex}}$.
³⁰W. A. Harrison, *Pseudopotentials in the Theory of Metals* (Benjamin, Reading, MA, 1966).
³¹U. Pustogowa, W. Hübner, K. H. Bennemann, and T. Kraft, Z. Phys. B **102**, 109 (1997).
³²O. Jepsen, J. Madsen, and O. K. Andersen, Phys. Rev. B **26**, 2790 (1982).
³³W. A. Harrison, *Electronic Structure and the Properties of Solids* (Freeman, San Francisco, 1980).
³⁴S. Müller *et al.*, Phys. Rev. Lett. **75**, 2859 (1995); A. P. Baddorf, A. K. Swan, and J. F. Wendelken, *ibid.* **76**, 3658 (1996); K. Robinson *et al.*, *ibid.* **76**, 3659 (1996); S. Müller *et al.*, *ibid.* **76**, 3660 (1996).
³⁵ θ denotes the angle between the magnetization direction z_M and the surface normal \hat{z} . ϕ is the angle between the x axis and the projection of z_M in the plane of the monolayer.
³⁶P. N. Argyres, Phys. Rev. **97**, 334 (1955).
³⁷Of course, SOC *itself* is part of a perturbation expansion, leading from the Dirac equation to the Pauli equation.
³⁸A. Lessard, Master's thesis, Freie Universität Berlin, 1996.
³⁹M. Farle *et al.*, Proceedings of E-MRS 1996 [J. Magn. Magn. Mater. (to be published)].
⁴⁰P. J. Jensen and K. H. Bennemann, Phys. Rev. B **42**, 849 (1990).
⁴¹A. McB. Collie and D. J. Powney, *The Mechanical and Thermal Properties of Solids* (Edward Arnold, London, 1973).
⁴²A. Dittschar *et al.*, J. Appl. Phys. **79**, 5618 (1996).
⁴³O. Eriksson (unpublished).
⁴⁴J. Trygg, B. Johansson, O. Eriksson, and J. M. Wills, Phys. Rev. Lett. **75**, 2871 (1995).
⁴⁵B. Újfalussy, L. Szunyogh, and P. Weinberger, Phys. Rev. B **54**, 9883 (1996). The authors show that even for Fe/Cu (001), the theory might have trouble reproducing the experimental results.
⁴⁶J. Dorantes-Dávila and G. M. Pastor, Phys. Rev. Lett. **77**, 4450 (1996). The authors calculate the in-plane magnetic anisotropy energy of Ni bcc(110) films. In the case of Ni(001), the situation is even more complicated, due to the higher symmetry of the (001) surface.